AIP Journal of Applied Physics

Optical transitions due to native defects in nonlinear optical crystals LiGaS2

A. Yelisseyev, Z. S. Lin, M. Starikova, L. Isaenko, and S. Lobanov

Citation: J. Appl. Phys. **111**, 113507 (2012); doi: 10.1063/1.4723645
View online: http://dx.doi.org/10.1063/1.4723645
View Table of Contents: http://jap.aip.org/resource/1/JAPIAU/v111/i11
Published by the American Institute of Physics.

Related Articles

From fabrication to mode mapping in silicon nitride microdisks with embedded colloidal quantum dots
Appl. Phys. Lett. 101, 161101 (2012)

Vanadium bound exciton luminescence in 6H-SiC
Appl. Phys. Lett. 101, 151903 (2012)

Broadband near-infrared emission from bismuth-doped multilayer films
J. Appl. Phys. 112, 073511 (2012)

Enhancement of carbon nanotube photoluminescence by photonic crystal nanocavities
Appl. Phys. Lett. 101, 141124 (2012)

Photoluminescence spectroscopy and energy-level analysis of metal-organic-deposited Ga2O3:Cr3+ films
J. Appl. Phys. 112, 063522 (2012)

Additional information on J. Appl. Phys.

Journal Homepage: http://jap.aip.org/
Journal Information: http://jap.aip.org/about/about_the_journal
Top downloads: http://jap.aip.org/features/most_downloaded
Information for Authors: http://jap.aip.org/authors

ADVERTISEMENT

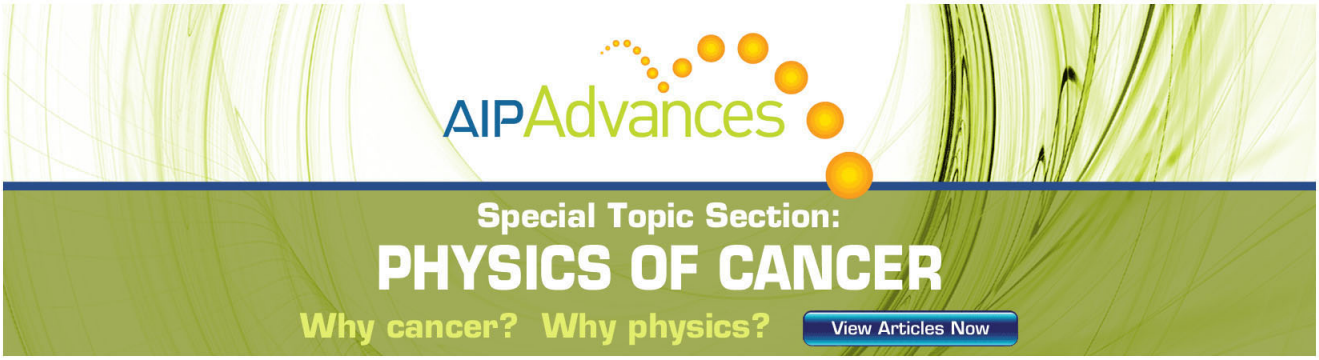

Downloaded 17 Oct 2012 to 62.141.173.103. Redistribution subject to AIP license or copyright; see http://jap.aip.org/about/rights_and_permissions

Optical transitions due to native defects in nonlinear optical crystals $LiGaS_2$

A. Yelisseyev,[1,a)] Z. S. Lin,[2,a)] M. Starikova,[1] L. Isaenko,[1] and S. Lobanov[1]
[1]*Institute of Geology and Mineralogy, Russian Academy of Sciences, Siberian Branch, 3 Academician Koptyug Avenue, Novosibirsk 630090, Russia*
[2]*Technical Institute of Physics and Chemistry, Chinese Academy of Sciences, Beijing 100190, China*

(Received 29 November 2011; accepted 30 April 2012; published online 4 June 2012)

$LiGaS_2$ (LGS) is a recently developed nonlinear optical crystal widely used for nonlinear conversion in the mid-infrared spectral region, but its applications are significantly influenced by the native defects present in the lattice. In this work, absorption and photoluminescence (PL) spectra are studied after annealing the as-grown LGS crystal in different chemical environments in order to reveal features related to anion vacancy (V_S) and cation antisite defect (Ga_{Li}). In addition, irradiation with fast electrons produces V_S centers and their complexes in LGS. The V_S migration and mutual transformations in these defects take place at room temperature whereas their complete annealing occurs at 670 K. Meanwhile, the first-principles calculations are adopted to identify the relevant optical transitions. A good agreement with the experimental results was obtained. It is established that the dominant defects V_S result in the optical absorption at 3.43 eV and violet PL emission, while Ga_{Li} is responsible for absorption at 2.95 eV. The intense PL peak at 1.92 eV is associated with the self-trapped excitons in LGS. The other weak PL bands are also related to the recombination of electrons or holes with the V_S and Ga_{Li} defect states. © *2012 American Institute of Physics*. [http://dx.doi.org/10.1063/1.4723645]

I. INTRODUCTION

Practical solid-state lasers generate wavelengths up to $\sim 3\,\mu m$, with the most prominent representatives in this limit being the fixed wavelength Er^{3+}-lasers and the tunable Cr^{2+}-lasers.[1] The spectral range above $3\,\mu m$ in the mid-IR can be continuously covered by nonlinear frequency down-conversion using powerful laser sources in the near-IR. Radiation in a spectral range up to about $4\,\mu m$ can be produced using oxide-based nonlinear crystals but at longer wavelengths they become opaque because of strong multi-phonon absorption. Most widely chalcogenide crystals such as $AgGaS_2$, $AgGaSe_2$, $HgGa_2S_4$, $ZnGeP_2$, GaSe, etc., are used in the mid-IR: they cover a range up to $20\,\mu m$ (Table I).[2] Since nonlinear frequency conversion is an intensity dependent process, high efficiency can be expected only when using pulsed laser sources (femtosecond to nanosecond). At practical pump intensities, most of the chalcogenide (non-oxide) mid-IR nonlinear crystals will suffer two-photon absorption (TPA) at the pump wavelength of 1064 nm because of their low bandgap. This is a serious constraint with regard to picosecond or nanosecond down-conversion devices for the mid-IR: optical parametric generators, amplifiers, and oscillators. Only few nonlinear crystals transparent in the mid-IR exhibit a bandgap corresponding to wavelengths shorter than 532 nm.[2] The situation is even more difficult in the femtosecond regime where one normally starts from 800 nm employing the Ti:sapphire lasers as pump sources, so it is necessary to use nonlinear optical crystals which are highly transparent near 400 nm in the second harmonic generation region.

Thus, the lithium ternary chalcogenides with the chemical formula $LiBC_2$, where B = In and Ga, C = S, Se, or Te, occupy a special position among the non-oxide nonlinear crystals because they are characterized by a minimum A^I cation size and lattice parameters which results in the strongest chemical bonds and largest bandgap E_g (Table I).[3,4] All members of this family were found to have the same wurtzite-type structure (space group *mm2*) except $LiGaTe_2$ which has a chalcopyrite lattice ($\bar{4}2m$).[5]

As a consequence, $LiBC_2$ compounds exhibit increased damage threshold and relatively low dispersion which is important for frequency conversion of short laser pulses. In addition, their thermal conductivity is higher than in their Ag analogues, so they have an essential advantage at high average powers. The $LiBC_2$ samples were obtained more than half a century ago[6] but their physical properties, especially those important for laser optics, were established much later when high quality crystals became available. Some of important parameters are given in Table I. Among the $LiBC_2$ compounds, $LiGaS_2$ (LGS) possesses the widest bandgap[3] and highest optical damage threshold at 1064 nm in the nanosecond regime,[4] although it exhibits relatively low nonlinear coefficients. Moreover, there was no surface deterioration observed even after periods of more than 5 yr. Its lowest dispersion and stability against gray track formation is indeed advantageous in optical parametric down-conversion of femtosecond pulses near 800 nm.[5]

The crystalline compound LGS was reported as early as 1947 in Ref. 6 where its average refractive index, density, and melting point were estimated. Hoppe identified its symmetry (β-$NaFeO_2$ type) and measured the lattice constants.[7] A precise structural study of brown-red color LGS was performed in Ref. 8. Single crystals of dimensions $4 \times 4 \times 5$ mm^3, of light yellow color, stable in air, were grown by the Bridgman–Stockbarger method.[9] Besides some physical properties, including micro-hardness and electric conductivity, the

[a)]Authors to whom correspondence should be addressed. Electronic addresses: elis@mail.nsk.ru and zslin@mail.ipc.ac.cn.

 © 2012 American Institute of Physics

Downloaded 17 Oct 2012 to 62.141.173.103. Redistribution subject to AIP license or copyright; see http://jap.aip.org/about/rights_and_permissions

TABLE I. Optical and thermal properties of the $LiBC_2$-type nonlinear crystals in comparison with AGS, ZGP, where nonlinear coefficients: d_{36} for AGS, ZGP, LGT and d_{24} for LIS, LISe, LGS, LGSe. Thermal conductivity is given for directions [100], [010], and [001], respectively.

Parameter	AGS	ZGP	LIS	LISe	LGS	LGSe	LGT
Transparency range (on 5 cm^{-1} level) (μm)	0.47-12.6	1.6-12.3	0.41-11.6	0.47-12.8	0.32-11.6	0.37-13.2	0.54-14.2
Band gap at 300 K (eV)	2.76	~1.8	3.57	2.86	3.65[a] 4.15[b] 3.93[c]	3.34	2.31
2nd order nonlinear susceptibility (pm/V)	13.4	75	5.7	8.2	5.1	7.7	43
Thermal conductivity at 300 K (W/(m K))	1.4, 1.1	35	6.2, 6.0, 7.6	4.7, 4.7, 5.5	…	…	…

[a]Reference 5.
[b]Reference 6.
[c]This work.

absorption edge at 330 nm (bandgap of 3.76 eV) was determined from transmission measurements at room temperature.[7] Kuryama grew light yellow LGS crystals with absorption edge at 340 nm (bandgap of 3.65 eV),[9] whereas Ohmer *et al.* gave 3.62 and 3.13 eV for LGS and LGSe, respectively.[10] Using the same technique,[11] we obtained the larger bandgap values $E_g = 4.15$, 3.34, and 2.3 eV, for LGS, LGSe, and LGT, respectively.[12] Bandgap values for Ag-containing analogues of these compounds are considerably lower 1.76, 1.83, and 1.316 eV for AGS, AGSe, and AGTe, respectively.[13] However, it should be emphasized that the practical application of these crystals is to a great extent dependent on the level of perfection of the growth technology and the achievable optical quality. Unfortunately, the growth of such crystals is complicated and deviation from stoichiometry is typical of the chalcogenides of the $LiBC_2$ family because of the high chemical activity of lithium and the sulfur volatility. Post-growth annealing in appropriate atmosphere is usually used to achieve the desired crystal composition and to approach the stoichiometric composition. Therefore, it is greatly desirable to study the role of defects in optical transitions in the ternary chalcogenides. Here, we report our investigations on the influences of the native point defects on the optical absorption and photoluminescence (PL) phenomena in the LGS crystal, by both the experimental and theoretical methods. These physical mechanism understandings and studied methods would be clearly applicable to the other important IR nonlinear optical crystals with the similar structural features.

The simplest defects which are present in as grown LGS crystals are anion vacancies V_S and cation antisite defects Ga_{Li}. Normally the valence of sulfur is -2, so the removing of a sulfur ion will leave two electrons unbounded in the lattice, forming the well-known F-center ($V_S^{2+} + 2e = V_S^0$).[14] In addition, Li ions are easy to be removed from the LGS lattices due to their high chemical activity and strong interaction with the container walls, whereas there is always an excess of Ga ions in the crystal. Taking into account the fact that the sizes of Li^+ and Ga^{3+} ions are 0.045 and 0.042 nm, respectively, the Ga_{Li} substitution is most likely to take place for the cation antisite defects in LGS. In this work, we systematically study the optical features of the sulfur vacancies V_S and the cation antisite defects Ga_{Li} in LGS by means of the optical spectroscopy and first-principles methods. A broad PL band peaked at 1.92 eV, observed in all LGS samples, was associated by a set of features with the self-trapped excitons. A strong 2.89 eV emission, excited mainly in the 3.4 eV absorption band in the sulfur deficient LGS, is related to the F-centers in the lattice. These defects form in LGS both at vacuum annealing and fast electrons irradiation. A broad absorption band at 2.95 eV in the transparency range but close to fundamental absorption edge is likely due to cation antisite defect Ga_{Li}. These experimental observations are in good agreement with the first-principles results, by which the mechanisms of the spectroscopic features of these native defects in LGS are elucidated.

II. EXPERIMENTAL METHODS

A. Crystal growth

The LGS single crystals were grown using the Bridgman-Stockbarger technique, in a double-zone vertical furnace. The upper and lower zones were separated by a diaphragm from heat-insulating material. The temperature of the melting zone was maintained at about 1420 K (roughly 100 K above the melting temperature). The axial temperature gradient was ~2 °C/mm. Typical rates of the ampoule sinking were 2 to 10 mm/day. The starting reagents were of 99.999% (Ga, S) and 99.9% (Li) purity. The charge was placed into a glass-graphite crucible and the latter was located in a silica ampoule. Such construction allows one to avoid the chemical reaction between lithium and the walls of the silica ampoule. The ratio between components in the charge was taken with some surplus (~0.2%) of Li and S relative to the $LiGaS_2$ composition so as to compensate the Li and S losses which are the most volatile components. The obtained LGS crystals were ~20 mm in diameter and ~50 mm in length. From the same as-grown boule, the (001) oriented plates were prepared, with thickness L of ~2 mm and apertures of ~0.5 cm^2. The plates were then annealed at ~1220 K in different atmospheres: in vacuum or in the presence of Li_2S, Ga_2S_3, and elementary S vapor. The vacuum annealing is expected to create new V_S defects in LGS, while the rich S or Ga vapor environment is expected to reduce the V_S content or affect the Ga_{Li} content in crystal. The annealed

Downloaded 17 Oct 2012 to 62.141.173.103. Redistribution subject to AIP license or copyright; see http://jap.aip.org/about/rights_and_permissions

LGS plates were polished for the spectroscopic studies. To estimate the bandgap, we prepared the LGS plate 60 μm thick: for such sample, it was possible to reach absorption coefficient values $\alpha \sim 10^3\,\mathrm{cm}^{-1}$ and to refine the band gap value estimated in Refs. 11 and 12. The ionizing irradiation with fast electrons was carried out on the linear electron accelerator in the Institute of Chemical Kinetics and Combustion, Novosibirsk. The electrons energy was 3.5 MeV and the dose was $\sim 10^{17}\,\mathrm{cm}^{-2}$. Crystals were cooled by flowing cold water during irradiation.

B. Spectroscopic studies

Absorption spectra for LGS were measured using a UV-2501PC Shimadzu spectrometer in the UV to near IR region and a Fourier transform spectrometer Infralum FT-801 in the mid IR. Spectra in the shortwave range were measured with a sample mounted in a metal cryostat with silica windows. Absorption coefficients were calculated from transmission measurements in the transparency region by use of the following formula:

$$T = (1-R)^2 e^{-\alpha d}/(1-R^2 e^{-2\alpha d}), \tag{1}$$

where α is the absorption coefficient (cm^{-1}), d the sample thickness (cm), and R the power reflection coefficient per surface. The R values measured using a technique of minimum deviation angle and the Sellmeier's equations for $R(\lambda)$ approximation were taken from Ref. 5. Measurements were carried out in unpolarised light and averaged $R(\lambda)$ values were used. An attempt was made to determine the dominant mechanism of band-to-band absorption for LGS at liquid nitrogen and room temperatures. This kind of transition is identifiable, in theory[11,15] at least, from the relationship between absorption α and the photon energy $h\nu$.

Thus $\alpha\, h\,\nu \propto (h\nu - E_g)^{1/2}$ for direct-allowed transitions and $\alpha\, h\,\nu \propto (h\,\nu - E_g)^2$ for indirect-allowed transitions. The band gap values are estimated by extrapolating the linear part of the $(\alpha h\nu)^2$ versus $h\nu$ or $(\alpha h\nu)^{1/2}$ versus $h\nu$ curves to $\alpha(h\nu) = 0$.

The PL spectra were recorded on diffraction luminescence spectrometer SDL1 with excitation from a 1 kW Xe lamp through a diffraction MDR2 monochromator. A cooled FEU83 photomultiplier sensitive up to 1.2 μm (1.03 eV) was used to detect the PL emission. The PL excitation (PLE) spectra were corrected to a constant amount of incident quanta using the Rhodamin 640 dye with permanent PL efficiency up to 550 nm.

III. THEORETICAL METHODS

The first-principles studies are performed using the plane-wave pseudopotential method[16] implemented in the CASTEP program.[17] The unit cell parameters and atomic positions of LGS were borrowed from Ref. 5. Ultrasoft pseudopotentials[18] are used with three valence electrons for Li ($1s^2 2s^1$), six for S ($3s^2 3p^4$), and thirteen for Ga ($3d^{10} 4s^2 4p^1$). A kinetic energy cutoff of 500 eV and the spin-polarised generalized-gradient approximation (GGA) with the Perdew, Burke, and Ernzerhof (PBE) exchange-correlation functional[19] is chosen for all the calculations. A large 128-atom supercell is used for all the point defect calculations, which is tested to be adequate for the current studies. Incorporation of a single Ga_{Li} impurity atom and a S vacancy results in an effective concentration of about 3.2 at. % and 1.5 at. %, respectively, close to the experimental conditions (see Sec. IV A). Brillouin-zone integrations are made using a $(2\times2\times2)$ k-point mesh (four irreducible k-points) according to the Monkhorst-Pack scheme.[20] The supercell volume and the atomic positions for the bulk are fully optimised using the quasi-Newton method with the Broyden, Fletcher, Goldfarb, and Shannon minimizer.[21] The convergence thresholds between optimization cycles for energy change, maximum force, maximum stress, and maximum displacement are set as 10^{-5} eV/atom, 0.03 eV/Å, 0.05 GPa, and 0.001 Å, respectively. The optimization terminates when all of these criteria are satisfied.

The formation energy of the point defect A of charge q is defined as

$$E_f(A,q) = E_{tot}(A,q) - E_{tot}(host) - \sum_i n_i\mu_i + q(E_F + E_v) + E_{corr}, \tag{2}$$

where $E_{tot}(A,q)$ is the total energy obtained from a supercell calculation with the point defect A, and $E_{tot}(host)$ is the total energy for the equivalent supercell containing just the host. n_i is the number of atoms of type i that have been added to ($n_i > 0$) or removed from ($n_i < 0$) the supercell as the defect is created from the host crystal, and μ_i is the corresponding chemical potentials of these species. Actually, the chemical potentials depend on the experimental growth conditions. Here, we only consider Ga-rich conditions ($\mu_{Ga} = E_{tot}$(bulk Ga)), the most extreme case for favoring formation of Ga_{Li} impurities and S vacancies, and the reservoirs with which S and Li atoms are exchanged with Ga_2S_3 and Li_2S are assumed. For both Ga_{Li} and V_S point defect species, the charge q is allowed to vary from 0 to +2. E_F is the Fermi level which is varied from the valence band maximum (VBM or E_v) to the conduction band minimum (CBM or E_c) in the bulk, i.e., $E_F \in [0, E_c\text{-}E_v]$, and $E_c\text{-}E_v$ is the band gap (E_g) of LGS. E_v is obtained from $E_v = E_{tot}(0, \text{host}) - E_{tot}(1+, \text{host})$, where $E_{tot}(0, \text{host})$ is the total energy of the neutral host supercell and $E_{tot}(1+, \text{host})$ is that of the 1+ charged host supercell.

As the formation energy directly obtained from the supercell model and GGA is an approximation, a correction term E_{corr} need to be included.[22,23] Normally, several corrections should be considered. They come from the GGA band gap error, the potential alignment, Makov-Payne interaction, and Moss-Burstein-like band filling effects.[23] However, it is found out that normally the formation energy modifications from the first correction could be in the order of several eV, while from the last three corrections are much smaller ($\sim$0.1 eV).[24] Therefore, in this work, the GGA band gap correction is considered only.

It is well known that GGA calculations usually underestimate the band gap E_g compared to experimental data. In this work, the calculated E_g of LGS is 3.41 eV which is smaller than the experimental value of 4.03 eV (see Sec. IV A), so

Downloaded 17 Oct 2012 to 62.141.173.103. Redistribution subject to AIP license or copyright; see http://jap.aip.org/about/rights_and_permissions

$\Delta E_g = E_g^{\text{Exp.}} - E_g^{\text{Cal.}} = 0.62\,\text{eV}$. A simple correction procedure is to shift the conduction bands (CB) upward to match the experimental E_g for donor-like defects or impurities, whereas the valence bands (VB) are kept fixed.[22,23] Meanwhile, the Ga_{Li} and V_S donor defects are also shifted with the CB, i.e., $E_{corr} = Z_e \Delta E_g$, where Z_e is the number of electrons at defect-induced donor levels in the band gap. For example, $Z_e = 2$ for Ga_{Li}^0 (or V_S^0), $Z_e = 1$ for Ga_{Li}^+ (or V_S^+), and $Z_e = 0$ for Ga_{Li}^{2+}(or V_S^{2+}).

The defect thermodynamic transition energy level (pinning energy) $\varepsilon_\alpha(q/q')$ is defined as the value of the Fermi level where the formation energy of defect (A,q) equals that of defect (A,q'), i.e.,

$$\varepsilon_\alpha(q/q') = [E_{tot}(A,q') - E_{tot}(A,q)]/(q' - q) - E_v. \quad (3)$$

This level would be observed in experiments where the final charge state can completely relax to its equilibrium configuration after the transition.[9,25] As defects are formed in a crystal, the following optical transitions involving the defect states must be considered:[23,26] photon absorption due to the excitation of an electron from (i) the VBM to the defect state or (ii) the defect state into the CBM, by which the charge state q of the defect changes by $+1$, and photon emission (luminescence) due to the decay of an electron from (iii) the CBM into the unoccupied defect state or (iv) the defect state into a hole (h) at the VBM, by which the charge state q of the defect changes by -1. The transition processes (i) and (ii) can be obtained by the optical absorption coefficients ε_2, i.e.,

$$\varepsilon_2(\hbar\omega) = \frac{2e^2\pi}{\Omega\varepsilon_0}\sum_{k,v,c} |\langle\psi_k^c|\hat{u}\cdot\vec{r}\,|\psi_k^v\rangle|^2 \delta(E_k^c - E_k^v - \hbar\omega), \quad (4)$$

where Ω is the volume of the elementary cell, v and c represent the VB and CB, respectively, ω is the frequency of the incident light, and $\hat{u}$ is the vector defining the polarization of the electric field of the incident light, which is averaged over the plane perpendicular to this direction. The photoluminescence (iii) and (iv), on the other hand, are directly determined by the optical level $\varepsilon_{opt}(q/q')$, which is defined similarly to the thermodynamic transition level, but the energy of the final state q' is calculated using the atomic configuration of the initial state q (i.e., account for the Franck-Condon shift).[23,26] Namely, for the photon emission (iii) which communicate with electrons (e)

$$\varepsilon_{opt}(q/q-1;e) = E_f(q-1) - E_f(q) - E_g, \quad (5)$$

where E_g is the (experimental) band gap energy. Similarly, for the photon emission (iv) which communicate with holes (h)

$$\varepsilon_{opt}(q/q+1;h) = E_f(q+1) - E_f(q). \quad (6)$$

Note that the PL energies are calculated as negative.

IV. RESULTS AND DISCUSSION

A. Bandgap and transmission|absorption spectra

The transmission spectra for LGS crystals annealed in different environments are shown in Fig. 1. At room temperature, all LGS samples are transparent in the 0.32-11.6 μm range above the transmission level of 10%, which corresponds approximately to the absorption level of 5 cm^{-1}. The short wave limit in the UV is determined by the fundamental absorption edge of LGS, whereas multiphonon absorption is responsible for the long wave limit: two-phonon absorption limits located at about 10 μm. The analysis of the shape of absorption spectra on a 60 μm thick LGS plate showed that the linear extrapolating is consistent with the $(\alpha h\nu)^2$ versus $h\nu$ curves, which corresponds to the case of direct-allowed band-to-band transitions (Fig. 2). This direct-allowed transition feature is also confirmed by the first-principles calculations.[27] Extrapolation of linear part to $\alpha(h\nu) = 0$ gives the E_g values 3.93 and 4.03 eV at 300 and 80 K, respectively. The 0.1 eV bandgap shift as temperature increases from 80 to 300 K is rather typical of wide-gap dielectrics.[28] The band gap of LGS was estimated as 4.15 eV at RT in the previous experiments,[12,13] in which the measurements were carried out on thick samples (L = 2 mm), and there was a strong ($\sim$20 cm^{-1}) absorption band centered at $\sim$330 nm near the fundamental absorption edge. To overcome this problem, in this work the considerably thinner plate with L = 60 μm is used, which allows us to measure absorption coefficients up to 10^3 cm^{-1}, and there are no strong bands in LGS samples under investigation. The intensity of high energy, near-edge absorption bands does not exceed 3 cm^{-1} value after background subtracting (Fig. 3). Therefore, the current E_g value is expected to be more accurate.

The main feature of the LGS transmission spectra (Fig. 1) is the occurrence of considerable optical losses in the 0.3 to 4 eV (0.3–5 μm) spectral region and a set of broad absorption bands near both shortwave and longwave transparency edges. The intensity of losses at $\lambda < 5$ μm correlated with the light scattering displays the monotonic decrease as the wavelength increases. Thus, at least a part of these losses is due to

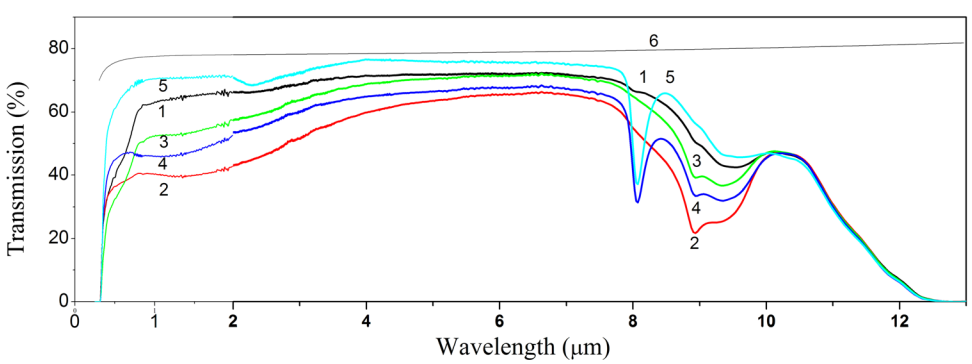

FIG. 1. Transmission spectra of the 2 mm thick LGS samples recorded at room temperature after annealing in different environments: as-grown LGS (1), in vacuum (2), and in the presence of vapors of Li_2S (3), Ga_2S_3 (4), and sulfur (5). Curve (6) shows the maximum possible transmission of LGS calculated using formula (1) by supposing zero absorption and multiple reflections. Reflection was calculated using the Sellmeier equations for LGS from Ref. 12.

Downloaded 17 Oct 2012 to 62.141.173.103. Redistribution subject to AIP license or copyright; see http://jap.aip.org/about/rights_and_permissions

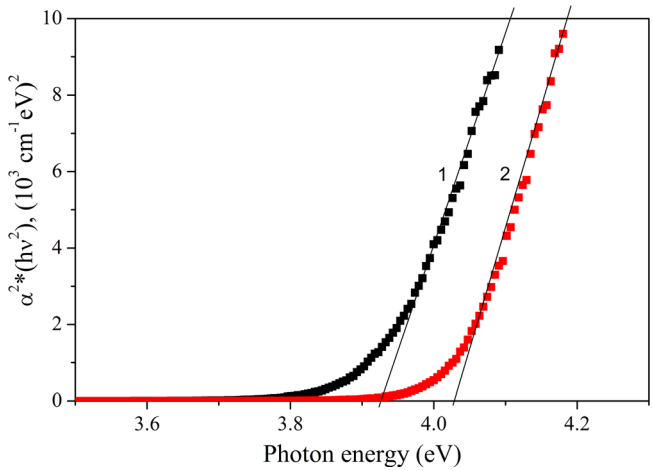

FIG. 2. Direct allowed transitions recorded on LGS plate with the thickness of 60 μm at (1) 300 K and (2) 80 K in which the E_g values are 3.93 and 4.03 eV, respectively.

the Rayleigh light scattering on the submicron inclusions of foreign phases. Indeed the intensity of nonresonant Rayleigh scattering is $\sigma \sim \lambda^{-4} r^6 (\varepsilon - \varepsilon_0)$, where r is the size of scattering particles (inclusions in our case) with $r \ll \lambda$, ε, and ε_0 the dielectric permittivity of scattering substance and the surrounding medium (crystal), so the scattering intensity is maximum at the short wavelength and decreases in the IR spectral region. Such optical losses are typically strong in the as-grown boules of ternary chalcogenides including $AgGaS_2$, $AgGaSe_2$, and $LiInS_2$; their as-grown boules are milky.[4,29] The other reason of such optical losses may be the optical absorption of dislocations which are known to produce a continuous set of levels in the forbidden zone.[30] A widespread technique to improve the transparency of an as-grown chalcogenide crystal is to anneal it in an appropriate atmosphere. In this work, we annealed the as-grown LGS crystals in vacuum and in S, Li_2S, and Ga_2S_3 environments, respectively: in these ways, we tried to affect the Li, Ga, and S contents in LGS. The transmission spectra of the as-grown and annealed LGS samples are given in Fig. 1. One may notice

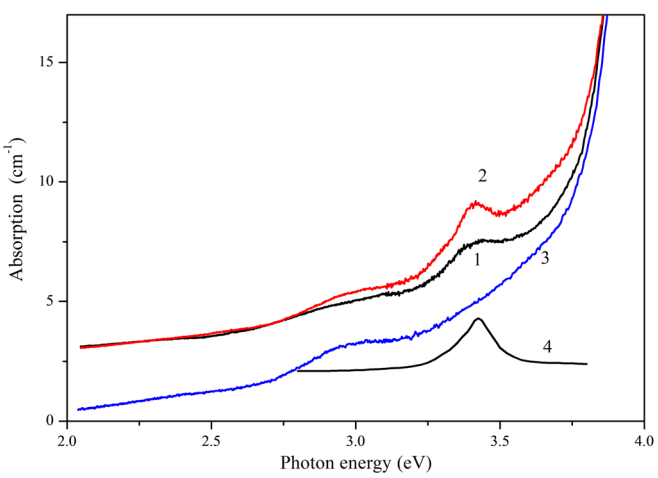

FIG. 3. Absorption spectra in the high energy spectral region recorded at 80 K for 2 mm thick as grown LGS plate (1) and for those after annealing at 950 °C in vacuum (2) and S vapor (3). Curve (4) is the differential spectrum from curves (2) and (3).

that the transmission of the as-grown LGS is relatively high: in the mid-IR region transmission $T = 70\%$, which is close to maximum transmission (up to 78%, curve (6)). Nevertheless, even in this case the optical losses are somewhat increased at shorter wavelengths. A weak residual absorption may be related to native or impurity point defects. The high transparency of the as-grown LGS means that actually its composition is close to the stoichiometric one. The absorption spectra for the LGS crystal annealed in the different atmospheres reveal that only the annealing in sulfur vapor improves the overall transparency in the as-grown LGS despite a strong optical absorption band at 8.0 μm and a much weak band centered at 2.5 μm. The other treatments, i.e., annealing in the vacuum, Li_2S and Ga_2S_3 environments, result in the increase of the Rayleigh scattering on submicron inclusions at short wavelengths[13] and produce a broad band at 9.3 μm with a narrower component at 8.9 μm, as shown in curves (2)–(4) in Fig. 1. In particular, the annealing in the vacuum significantly decreases the transparency of the as-grown LGS. The 8.9/9.3 μm component is known to be related to the Ga-O vibrations,[31] revealing that there has trace of oxygen contamination in the LGS crystal. In addition, after annealing in the Ga_2S_3 vapors, another strong absorption band at 8.0 μm appeared, similar to the case of annealing in S vapor. This absorption band is associated with the S-S vibration, which is also observed in the chalcogenide glass.[31] All the above measurements demonstrate that the annealing in sulfur, Li_2S, and Ga_2S_3 atmospheres does compensate the existing deficit in S or even create the surplus. The occurrence of S-S vibrations indicates that some sulfur atoms are in the close adjacent positions. Since there are no such S pairs in the perfect LGS structure, this means that some S atoms occupy the interstitial positions or cation (Li or Ga) sites. Taking into account that the 8.0 μm absorption band appears only after annealing in Ga_2S_3 (not in Li_2S), one may conclude that S is more likely to occupy the Li site (not Ga site). This result is consistent with the fact that the size of Li (0.045 nm) is somewhat larger than that of Ga (0.042 nm), so the S anions (0.184 nm) are more favored to replace the lithium sites.

Fig. 3 shows the absorption spectra on the short wavelength side for the as-grown LGS crystal (curve (1)) and LGS after annealing in the vacuum (curve (2)). Clearly, two broad absorption bands are observed around 3.43 and 2.95 eV in photon energy scale (or around the wavelengths of 375 and 420 nm, respectively); they are more pronounced at low temperatures. The intensity of the 3.43 eV band present in as-grown LGS samples increases after annealing in vacuum (curve (2)), but this band disappears completely after annealing in the sulfur vapor (curve (3)), which can be clearly displayed by the differential spectrum (curve (4)) obtained by subtracting the curve (3) from the curve (2). Such behavior allows us to associate the 3.43 eV band with a sulfur vacancy (F-center). On the other hand, the 2.95 eV band present in all of the samples is almost independent of the annealing treatments, which is related to the cation antisite defect, Ga_{Li}. The absorption phenomena are further studied from the first-principles calculations in Sec. IV C. Based on the above optical absorption spectra, one may see that the

Downloaded 17 Oct 2012 to 62.141.173.103. Redistribution subject to AIP license or copyright; see http://jap.aip.org/about/rights_and_permissions

annealing in vacuum or sulfur vapor is a convenient technique to control the LGS transparency in the visible and near-IR spectral region.

The defect concentration N can be estimated from the absorption spectrum, using the well known Smakula's formula[32]

$$N(\mathrm{cm}^{-3}) = 0.821 \times 10^{17} \times (n/(n^2+2)^2) \times (1/f_{ij}) \times \int \alpha(E)\mathrm{d}E, \quad (7)$$

where n is the refractive index for LGS in the environment of the absorption bands, f_{ij} is the oscillator's strength, $\alpha(E)$ is the absorption coefficient (cm^{-1}), and E is the photon energy (eV). For the Gaussian case, which takes place in LGS, formula (7) transforms to

$$N(\mathrm{cm}^{-3}) = 0.87 \times 10^{17} \times (n/(n^2+2)^2) \times (1/f_{ij}) \times \alpha_{\max} \times \gamma, \quad (8)$$

where $\alpha_{\max}$ is the maximum absorption and γ is the full width at half maximum (FWHM) of the absorption band (eV). According to Ref. 12, $n \sim 2.3$ at the photon energy about 3 eV for LGS. The FWHMs of the optical absorption bands around 3.43 and 2.95 eV are 0.16 and 0.31 eV, and $\alpha_{\max} = 2.0$ and $0.9\,\mathrm{cm}^{-1}$, respectively. Therefore, the estimated defect concentration $N(3.43\,\mathrm{eV}) = 7.3 \times 10^{18}/f$ and $N(2.95\,\mathrm{eV}) = 0.37 \times 10^{18}/f$. Taking $f = 0.1$, which is the typical oscillator strength for F centers in LiF and NaF,[33] the defect concentrations N are about $10^{19}\,\mathrm{cm}^{-3}$ for both 3.43 and 2.95 eV bands.

F-centers are known to form not only at vacuum annealing or additive coloration but also at ionizing irradiation. Radiative defect formation is well studied in elemental semiconductors (Si, Ge, diamond) and binary compounds (alkali halides, oxides, chalcogenides) in connection with multiple applications.[32] There is much less information on multicomponent compounds including ternary chalcogenides. Low-temperature ionizing irradiation produces different Frenkel defects such as vacancies and interstitials as well as their complexes,[34] but mainly anion vacancies remain at room temperature. Fig. 4(a) shows that the absorption spectra of LGS before and after electron irradiation as well as after annealing during 5 min at different temperatures in the range of 300 to 620 K are given. One can see that strong absorption at $h\nu > 1.7$ eV appears after such irradiation. It weakens as crystal is warmed step by step and disappears completely near T = 670 K. We further separate three individual bands in the LGS spectrum, which are given in the insert in Fig. 4(a). A superposition of these bands produces the resulting absorption spectra of irradiated LGS. The maximums of these bands are located at 2.0, 2.65, and 3.4 eV. The latter band is in the most intense and is ~2 orders stronger than the 2.0 eV component. This intense band at 3.4 eV in irradiated LGS is almost the same as the absorption band 3.43 eV in LGS after annealing in vacuum (Fig. 3). Thus, the F-centers and some other point defects are produced at irradiation. Temperature dependence for these three components titled as A, B, and C, respectively, is given in Fig. 4(b). We find that the intensity of two bands, at 3.4 and 2.0 eV, decreases

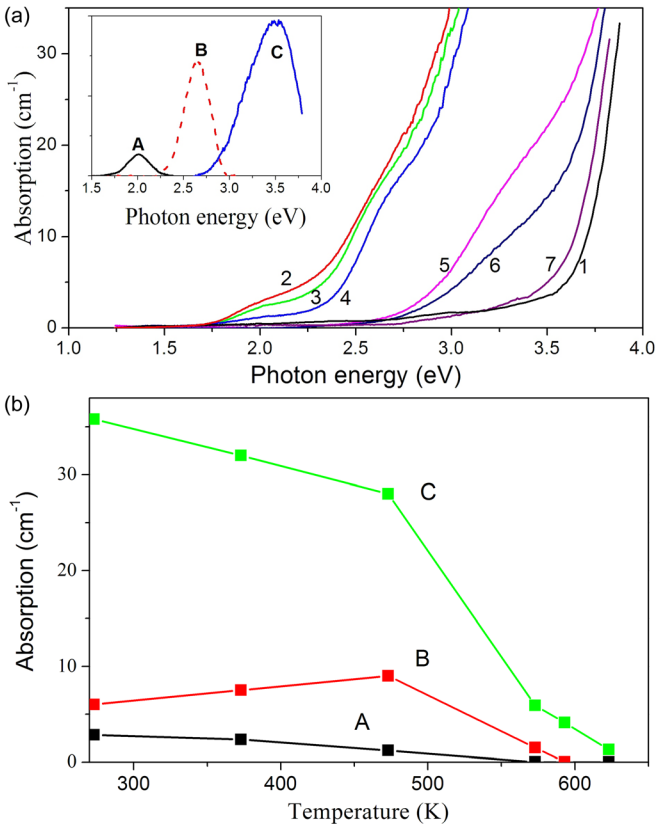

FIG. 4. (a) Absorption spectra of LGS single crystals before (1) and after (2) irradiation with 3.5 MeV electrons. Spectra 3-7 show absorption spectra after further annealing of irradiated LGS during 5 min at 370, 470, 570, 600, and 620 K, respectively. Individual components A, B, and C in the absorption spectrum of irradiated LGS are given in the insert. All spectra were recorded at T = 300 K. (b) Temperature dependence of absorption in individual components at 2.0 eV (A), 2.65 eV (B), and 3.5 eV (C) at isochronic annealing. Absorption was measured in the band maximum for bands A, B and in the low energy wing (at $h\nu = 3.0$ eV) for C band. Since the absorption is too intense for spectra 2-4, these spectra were measured only to 3.0 eV photon energy which corresponds to a wing of the 3.4 eV band (C band).

steadily as annealing temperature grows, whereas the 2.65 eV component demonstrates a maximum near 470 K. The inclination of annealing curves for 3.4 and 2.0 eV components near room temperature in Fig. 4 implies that the anion vacancies are moveable and some defect transformations take place in LGS at this temperature. The build-up of the 2.65 eV band near 470 K during annealing is likely due to F-centers aggregation and some complexes, probably F_2.

B. Photoluminescence and PL excitation spectra

Low-temperature (80 K) PL spectra for as-grown LGS, recorded at 4.13 eV (300 nm) and 3.4 eV (365 nm) excitations, are given in Fig. 5. The shortwave excitation produces a relatively intense yellow-reddish PL in a broad band centered at 1.92 eV (~650 nm) with FWHM = 0.56 eV (Fig. 5(a)): this emission becomes ~4 times weaker as temperature increases from 80 to 300 K. Meanwhile, the 3.4 eV light excitation produces an intense violet PL centered at 2.89 eV (~425 nm) and three other weaker individual components located at 2.45 eV (~505 nm), 1.92 eV (~650 nm), and 1.34 eV (~925 nm), respectively (Fig. 5(b)). Their corresponding FWHM values are 0.23, 0.29, 0.52, and 0.17 eV,

Downloaded 17 Oct 2012 to 62.141.173.103. Redistribution subject to AIP license or copyright; see http://jap.aip.org/about/rights_and_permissions

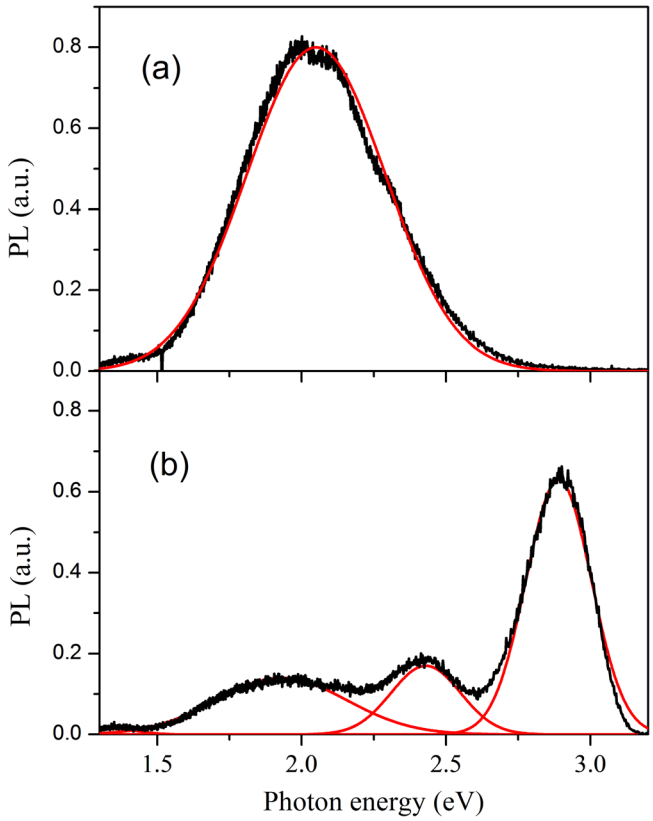

FIG. 5. PL spectra recorded for LGS at 80 K with the excitation energy of 4.13 eV (a) and 3.4 eV (b). The decomposed Gaussians are displayed by the red thin solid lines (one component for (a) and four components for (b)).

and they depend weakly on temperature. The PL spectrum remains the same as one lowers the temperature from 80 to 4.2 K: no fine structure appears. This means that the case of strong electron-phonon interaction is realized. The shape of the absorption/emission bands is close to Gaussian in this case. The PL spectrum in Fig. 5(b) is decomposed into Gaussians by the thin solid lines. Two high-energy PL components (dominating peak at 2.89 eV and a weaker component at 2.45 eV) are quenched only partly (~30%) as temperature increases to room temperature. However, the post-growth annealing affects considerably these two PL components: annealing in vacuum increases their intensity, whereas annealing in sulfur containing vapor (in the presence of solid Li_2S, Ga_2S_3, or S) quenches this PL up to complete disappearance. Therefore, these PL bands have similar behaviour and are closely associated with the same defect: sulfur vacancies V_S. On the other hand, annealing in different atmospheres does not affect the intensity of the 1.92 eV emission peak.

If the PL emission wavelength is fixed and the excitation wavelength is scanned, one obtains the PLE spectrum after correction for the spectral distribution of the Xe lamp source. This spectroscopy gives information about the absorption spectrum of the luminescence center even when its contribution to the absorption spectrum recorded in the common way is very weak. Fig. 6 shows PLE spectra for the main PL emissions in LGS. One can see that intense violet PL (2.89 eV) related to V_S is excited most effectively in the 3.4 eV band in the LGS transparency range, whereas at band-to-band transitions $h\nu > 4\,\text{eV} \sim E_g$ its intensity is much weaker. The Stokes shift changes slightly with temperature: it is 0.51 and 0.53 eV at 80 K and 300 K, respectively. A relative estimate for the Huang-Rhys factor (S, average number of participating phonons) can be obtained on the basis of a semiclassical configuration coordinate diagram.[35] With the assumption of parabolic potential curves and equal ground- and excited-state effective vibration frequencies, the low-temperature Stokes shift is given as $\Delta = E_{abs} - E_{em} = \hbar\omega(2\,S\text{-}1)$. Insertion of experimental quantities including maximum phonon energy $\hbar\omega \sim 300\,\text{cm}^{-1}$ for LGS (Ref. 12) yields $S = 5$ to 6.5 for sulfur vacancy.

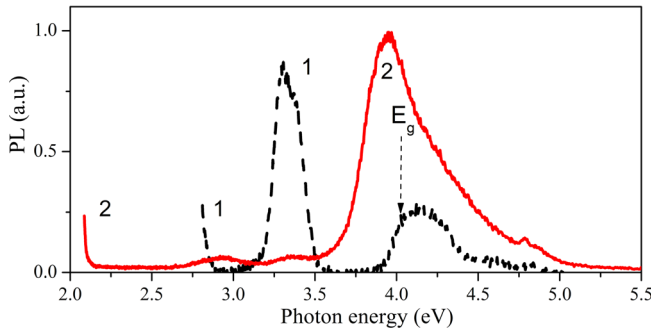

FIG. 6. PLE spectra at 80 K for emissions $h\nu = 2.8$ (1) and 1.8 eV(2) in LGS after annealing in vacuum. The arrow shows the band gap (4.03 eV) at 80 K.

The PLE spectrum for yellow-reddish emission in the 1.92 eV band is a broad band, the intensity of which grows quickly as photon energy increases, beginning from 3.6 eV and reaches maximum at 3.95 eV, close to the band gap (4.03 eV). For this emission, the separation of PL band from the main excitation band is 2.03 eV and 1.74 eV at 80 K (Figs. 5 and 6). S values are of about 20 for this emission. The PL decay time of 1.92 eV emission is in the microsecond range as follows from the PL experiments by Pustovarov using synchrotron radiation on the SUPERLUMI station. Large width of the emission band, excitation near fundamental absorption edge, a large Stokes shift (>1 eV), strong temperature dependence, and μs decay time are the properties, which are typical of self-trapped excitons (STE) in other wide gap materials.[36,37] For example, the Stokes shifts Δ determined for STE emission are 1.0 eV for TiO_2,[36] 1.4 eV for α-Al_2O_3,[37] 2.35 eV for Y_2O_3,[37] whereas for alkali halides Δ varies from 1.5 to 5.5 eV.[38] Thus, the 1.92 eV emission of LGS might be attributed to the radiative decay of self-trapped excitons (triplet-singlet transitions). Correspondingly, the 3.95 eV peak in PLE spectra may be related to the formation of the excitons and tens of phonons are burned at exciton self-trapping. The emission of free excitons was observed at temperatures as low as 5 K in ternary chalcogenides such as $AgGaS_2$ and $AgGaSe_2$ and even stimulated emission was obtained on these transitions.[39] Self-trapped excitons were reported also for crystalline As_2S_3 and Se.[40] Nevertheless even at 4.2 K, we found in PL spectra of LGS no fine structure which could be related to free excitons.

It is noteworthy that Stokes shift value is low enough $\Delta = 0.5$ eV for F-centers in LGS. One can compare this value with $\Delta \sim 1.4$ to 2.5 eV for alkali halides,[32] ~2 eV for Al_2O_3

Downloaded 17 Oct 2012 to 62.141.173.103. Redistribution subject to AIP license or copyright; see http://jap.aip.org/about/rights_and_permissions

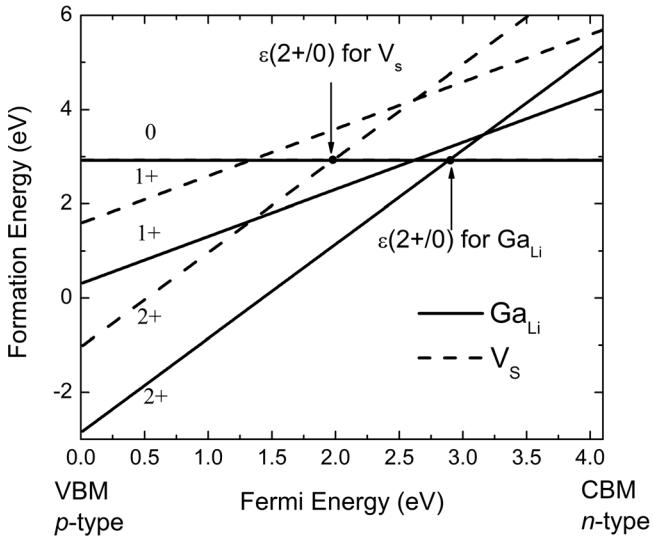

FIG. 7. Formation energy of the different charge states of Ga_{Li} and V_S in LGS, as a function of the Fermi level E_F within the band gap.

(Ref. 40) and $\Delta \sim 0.5$ eV for GR1 system, corresponding to neutral vacancy in diamond.[41] The $\Delta/2$ values are considered as a polaron energy in solids,[42] thus characterizing a degree of bond covalence. The latter increases from alkali halides to diamond and it is large enough in LGS.

C. *Ab initio* results on defect states and optical transitions

Fig. 7 shows the calculated formation energy of the different charge states of Ga_{Li} and V_S in LGS, as a function of the Fermi level E_F within the band gap. It can be seen that for both defects, the 2+ charge state and neutral charge state are most stable in the region close to VBM and CBM, respectively. Moreover, both the first thermodynamic transition state $\varepsilon(+/0)$ is deeper (farther from the CBM) than the second transition energy $\varepsilon(2+/+)$, leading to a $\varepsilon(2+/0)$ transition from the 2+ state directly into the neutral state. This means the effective correlation energy U, defined as the difference between the relevant transition levels, i.e., $U = \varepsilon(+/0) - \varepsilon(2+/0)$, is negative. This behavior of negative U energy is directly associated with the large lattice relaxations in the neutral and in the fully ionized (2+) states. For Ga^0_{Li}, the distances between the substituted Ga and the nearest neighbor (NN) S atoms are about 2.76 Å, which decrease to about 2.33 Å in the 2+ states. For V^0_S and V^{2+}_S, the distances to the NN Ga atoms close to the sulfur vacancy are 2.74 Å and 5.04 Å, respectively. The calculated $\varepsilon(2+/0)$ thermal transition levels are located at $E_v + 2.84$ eV and $E_v + 1.91$ eV for Ga_{Li} and V_S, respectively, both quite deep in the band gap. Therefore, the equilibrium stable configurations of both defects are not expected to provide the high free-carrier concentration for the n-type doping.

The electronic structures for the perfect LGS and those containing the Ga_{Li} or V_S defects are displayed in Fig. 8 by the partial density of states (PDOS) projected on atom species. In perfect LGS (Fig. 8(a)), the s and p orbitals on Ga and S are located at the edge of band gap and exhibit strong hybridizations, but their interaction with the orbitals

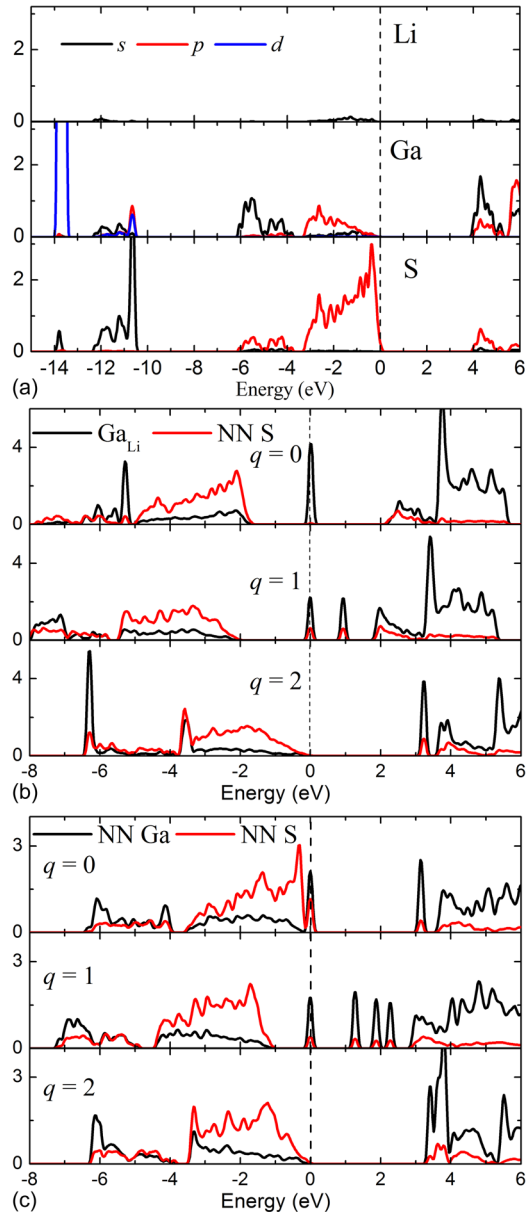

FIG. 8. Calculated PDOS of a perfect LGS crystal(a), and those of the neutral ($q = 0$) and charged ($q = 1$ and 2) cation antisite defects Ga_{Li} and the NN S atom (b), and the atoms surrounding the neutral and charged sulfur vacancy V_S(c). The vertical dashed lines indicate the Fermi levels.

on lithium is weak. In addition, the localized Ga 3d orbitals are quite deep in the VB (at about -13 eV), and the Li 1s orbitals are much deeper at -48 eV (not shown). As the Ga_{Li} and V_S defects are formed in the lattice, the PDOS on the Ga and S atoms NN to the single-point defect are significantly modified, but on the next-nearest neighbor quickly recovers to the perfect situation. For the neutral Ga_{Li} defect ($q = 0$), a substitutional Ga atom provides two excess electrons on the Li site and pushes the NN S atom outward due to the Coulomb repulsion. The electrostatic interaction results in the occurrence of double degenerate defect state in the band gap, which is mainly composed of the Ga_{Li} 4s orbitals (upper panel in Fig. 8(b)). In the Ga^+_{Li} configuration ($q = 1$, middle panel in Fig. 8(b)), the defect state is occupied by one electron and moves to the position near the CBM. In the Ga^{2+}_{Li} case ($q = 2$, lower panel in Fig. 8(b)), the defect state is

Downloaded 17 Oct 2012 to 62.141.173.103. Redistribution subject to AIP license or copyright; see http://jap.aip.org/about/rights_and_permissions

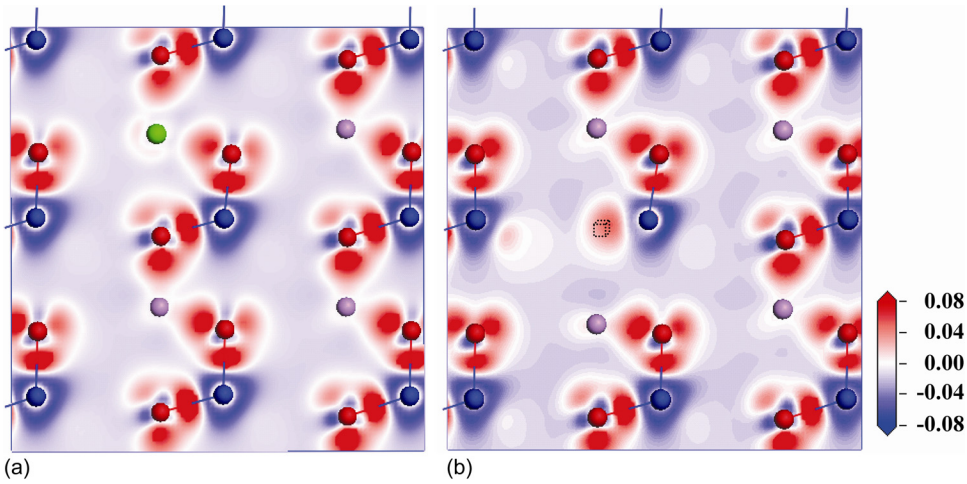

FIG. 9. Charge-density difference maps around the neutralized defects for (a) Ga_{Li} and (b) V_S. The slices are taken perpendicular to the *b*-axis and pass through the defects. The Li, Ga, and S atoms are represented by the cyan, blue, and red balls, respectively. The Ga_{Li} atom is represented by the green ball, and the S vacancy is indicated by a dashed box. The color level goes from a reduction in density (blue) to a gain in density (red) and the units are e/Å^2.

completely unoccupied, and the NN S atoms strongly relax inward so that their distances to the substitutional Ga atom are within 2% compared to the perfect Ga-S bond lengths in LGS. This relaxation forms a strong chemical bonding between the Ga_{Li} and S atoms, and the empty defect state is located just below the CBM, significantly reducing the formation energy of Ga_{Li}^{2+} with respect to Ga_{Li}^{+}. For the V_S case, the atomic relaxation feature and electronic characteristics are similar (Fig. 8(c)); the removal of a sulfur atom from the host crystal leaves two Ga dangling bonds, and their large relaxation from V_S^0 to V_S^{2+} configuration strengthens the surrounding Ga-S bonds, making the sulfur vacancy a negative-U center.

Figs. 9(a) and 9(b) display the charge-density difference contour maps around the neutralized V_S and Ga_{Li} defects, respectively. The charge redistribution is determined by subtracting the valence charge density of the whole system from that of the respective free atoms. It is clear that a large direction dependent redistribution of the charges between the S and Ga ions takes place, indicating the obvious character of covalent chemical bonding. Meanwhile, the electron transfer around the Li atom is quite small. As the native point defects Ga_{Li} or V_S are present, the modification of the charge-density redistribution is quite localized: a few electrons accumulate in the defect sites. So it has tendency to push the antisite defect Ga_{Li} and the NN S anion apart, but to pull the sulfur vacancy V_S and the NN Ga cation together.

Based on the neutral electronic band structures, the optical absorption spectra of the LGS with the Ga_{Li} or V_S defects are obtained from formula (4). These spectra are shown in Fig. 10, where absorption of the perfect LGS is also displayed for comparison. It is clearly shown that the Ga_{Li} defect results in the absorption peak centered at about 2.7 eV (~460 nm, curve (2)), while the Vs defect causes the absorption around 3.2 eV (~380 nm, curve (3)). They are in good agreement with the experimental measured values of 2.95 and 3.43 eV, respectively. The shift of the experimental absorption peak ~0.1 eV to high energies may be a result of a steep increase in absorption in the background or some polarization effects. Furthermore, the relative absorption intensity of the two peaks in the absorption spectra is also in a very good prediction, so the overall calculated spectrum (curve (4)) agrees with the experimental results (curve (5)) very well. Therefore, our first-principles calculations confirm that the Ga_{Li} and V_S defects are the dominant native point defects in LGS and result in the optical absorption in the visible spectral region.

We also calculated the PL emission energies for the Ga_{Li} or V_S defects and compared them with the experimental PL results (Fig. 5). This allowed us to interpret the experimental observations in the following way: Upon photoexcitation, the electrons in the occupied defect states of V_S^0 (or Ga_{Li}^0) are promoted into the states close to the CBM, i.e., the perturbed-host state (PHS),[26,43] creating the ionized state V_S^{2+} (or Ga_{Li}^{2+}). The radiative recombinations of the electrons from the PHS into the defect-localized states cause the violet emission at 2.89 eV (for V_S^{+}), whereas recombination in Ga_{Li}^{+} is nonradiative. In fact, the origin of the violet emission phenomenon is also confirmed in the PL experiments by annealing the as-grown LGS crystal in the vacuum and sulfur

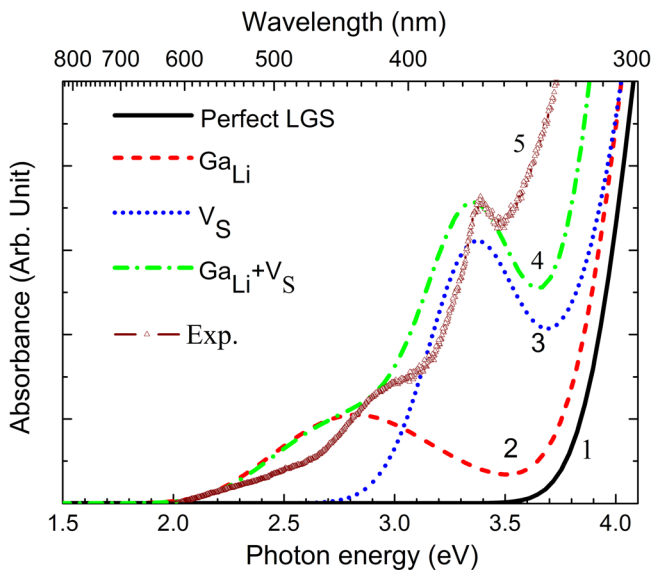

FIG. 10. Calculated optical absorption spectra for perfect LGS (1) and for the samples with anion vacancies V_S (2) and cation antisite defects Ga_{Li} (3). Curve (4) demonstrates a combined absorption from both defects (the sum of curves (2) and (3)). The experimental data are displayed in curve (5) for a comparison.

Downloaded 17 Oct 2012 to 62.141.173.103. Redistribution subject to AIP license or copyright; see http://jap.aip.org/about/rights_and_permissions

environment (see Sec. IV B). For the yellow-red emission at 1.94 eV dominantly generated from the self-trapped excitons, there have some contributions from the optical transition $V_S^{2+} + e \rightarrow V_S^{+}$ and $Ga_{Li}^{2+} + e \rightarrow Ga_{Li}^{+}$, in which the corresponding theoretical optical transition level $\varepsilon_{opt}(2+/+, e) = -1.84$ eV and -1.73 eV, respectively. This may explain the observation that the FWHM value of this PL band is about 2 times larger than that of the other PL bands.

Meanwhile, the photon emission can be generated by the decay of holes at VBM into the defect-localized states as well. Our calculations reveal that the optical transition level $\varepsilon_{opt}(+/2+, h) = -2.33$ eV for the process $Ga_{Li}^{+} + h \rightarrow Ga_{Li}^{2+}$ and $\varepsilon_{opt}(0/+, h) = -1.71$ eV for the process $Ga_{Li}^{0} + h \rightarrow Ga_{Li}^{+}$. These energies are consistent with the observed PL peaks at 2.45 and 1.92 eV, respectively. For the near-IR emission at 1.34 eV, the optical process $V_S^{+} + h \rightarrow V_S^{2+}$ corresponds to this transition, with the theoretical $\varepsilon_{opt}(+/2+, h) = -1.35$ eV. It should be noted that the PL phenomena involving the hole combinations are much weaker than those involving the electron combinations, which is clearly verified in Fig. 5(b) by the fact that the intensity of 1.34 eV peak is an order weaker than that of the others. In addition, we predict that there exists another weak IR emission at 0.54 eV ($\sim$2290 nm) due to the transition $V_S^{0} + h \rightarrow V_S^{+}$.

V. CONCLUSIONS

The optical transitions due to the native point-defects V_S and Ga_{Li} in LGS are studied by the absorption and photoluminescence spectroscopy, combined with the first-principles calculations. Irradiation with fast electrons with 3.5 MeV energy produces V_S centers and their complexes in LGS. The V_S migration and mutual transformations in these defects take place at room temperature, whereas their complete annealing occurs at 670 K. The as-grown LGS crystals are annealed in vacuum, and in the vapors of sulfur, Ga_2S_3 and Li_2S, in order to modify the defect concentration in the lattice. It is revealed that the transmission in LGS is improved after annealing in sulfur vapor. The V_S are the main native point defects, and their content increases at annealing in vacuum and per contra decreases at annealing in the presence of sulfur-containing vapors. These anion vacancies are responsible for the optical absorption band at 3.43 eV and intense violet PL at 2.89 eV. The Ga_{Li} defects, on the other hand, are not easily removed from the lattices, and result in the optical absorption band at 2.95 eV. The intense PL at 1.92 eV is dominantly associated with the self-trapped excitons in LGS. A weak PL peak at 1.34 eV is caused by the decay of holes into the V_S defect states. We believe that these identifications are important for understanding the role of defects in the optical transition processes in LGS and also have implications on the studies of similar optical phenomena in other optical crystals.

ACKNOWLEDGMENTS

This work was supported by the NSF (Nos. 91022036 and 11174297), 973 project (Grant Nos. 2010CB630701 and 2011CB922204) of China, and the Special Foundation of the President of the Chinese Academy of Sciences as well as by the Russian Foundation of Basic Research (Grant No 11-02-00817).

[1]A. A. Kaminskii, Laser Photonics Rev. **1**, 93 (2007).
[2]V. Petrov, F. Noack, I. Tunchev, P. Schunemann, and K. Zawilski, Proc. SPIE **7197**, 71970M (2009).
[3]L. Isaenko, A. Yelisseyev, S. Lobanov, P. Krinitsin, V. Petrov, and J.-J. Zondy, J. Non-Cryst. Solids **352**, 2439 (2006).
[4]J.-J Zondy, V. Petrov, A. Yelisseyev, L. Isaenko, and S. Lobanov, in *Mid-Infrared Coherent Sources and Applications, NATO Science for Peace and Security Series—B: Physics and Biophysics*, edited by M. Ebrahim-Zadeh, and I. Sorokina, (Springer, 2008), p. 67.
[5]L. Isaenko, I. Vasileva, A. Merkulov, A. Yelisseyev, and S. Lobanov, J. Cryst. Growth **275**, 217 (2005).
[6]B. N. Ivanov, A. I. Emin, and Ya. I. Rabovik, J. Gen. Chem. (USSR) **17**, 1247 (1947).
[7]R. Hoppe, Bull. Soc. Chim. Fr. **1965**, 1115 (1965).
[8]J. Leal-Gonzales, S. S. Melibary, and A. J. Smith, Acta Crystallogr. **C46**, 2017 (1990).
[9]Z. Z. Kish, V. V. Loshak, E. Yu. Peresh, and E. E. Semrad, Inorg. Mater. **25**, 1258 (1989).
[10]M. C. Ohmer, J. T. Goldstein, D. E. Zelmon, A. W. Saxler, S. M. Hedge, J. D. Wolf, P. G. Schunemann, and T. M. Pollak, J. Appl. Phys. **86**, 94 (1999).
[11]G. C. Bhar and R. C. Smith, Phys. Status Solidi **13A**, 157 (1972).
[12]L. Isaenko, A. Yelisseyev, S. Lobanov, A. Titov, P. Krinitsin, V. Vedenyapin, and J. Smirnova, Cryst. Res. Technol. **38**, 379 (2003).
[13]G. C. Catella and D. Burlage, MRS Bull. **23**, 28 (1998).
[14]W. Hayes and A. M. Stoneham, *Defect and Defect Processes in Nonmetallic Solids* (Wiley, New York, 1985).
[15]T. S. Moss, *Optical Properties of Semiconductors* (Butterworth, London, 1961).
[16]M. C. Payne, M. P. Teter, D. C. Allan, T. A. Arias, and J. D. Joannopoulos, Rev. Mod. Phys. **64**, 1045 (1992).
[17]S. J. Clark, M. D. Segall, C. J. Pickard, P. J. Hasnip, M. J. Probert, K. Refson, and M. C. Payne, Z. Kristallogr. **220**, 567 (2005).
[18]D. Vanderbilt, Phys. Rev. B **41**, 7892 (1990).
[19]J. P. Perdew, K. Burke, and M. Ernzerhof, Phys. Rev. Lett. **77**, 3865 (1996).
[20]H. J. Monkhorst and J. D. Pack, Phys. Rev. B **13**, 5188 (1976); Phys. Rev. B **16**, 1748 (1977).
[21]T. H. Fischer and J. Almlof, J. Phys. Chem. **96**, 9768 (1992).
[22]C. Persson, Y. J. Zhao, S. Lany, and A. Zunger, Phys. Rev. B **72**, 035211 (2005).
[23]S. Lany and A. Zunger, Phys. Rev. B **78**, 235104 (2008).
[24]C. G. Van de Walle and J. Neugebauer, J. Appl. Phys. **95**, 3851 (2004).
[25]S. B. Zhang, J. Phys.: Condens. Matter **14**, R881 (2002).
[26]S. Lany and A. Zunger, Phys. Rev. B **72**, 035215 (2005).
[27]L. Bai, Z. S. Lin, Z. Z. Wang, and C. T. Chen, J. Appl. Phys. **103**, 083111 (2008).
[28]J. Aarik, H. Mandar, M. Kirm, and L. Pung, Thin Solid Films **466**, 41 (2004).
[29]R.-M. Nigge, F. P. Baumgartner, and E. Bucher, Sol. Energy Mater. Sol. Cells **43**, 335 (1996).
[30]L. Bonch-Bruevich and V. B. Glasko, Sov. Phys. Solid State **3**, 26 (1961).
[31]V. F. Kokorina, *Glasses for Infrared Optics* (CRC, Boca Raton, FL, 1996), p. 236.
[32]W. B. Fowler, *Physics of Color Centers* (Academic, New York, 1968), Chaps. 2 and 6.
[33]A. Lusschik, M. Kirm, Ch. Luschik, I. Martinson, and G. Zimmerer, J. Lumin. **87**, 232 (2000).
[34]Ch. B. Lushchik and A. Ch. Lushchik, *Decay of Electronic Excitations with Defect Formation in Solids* (Nauka, 1989), p. 264 (in Russian).
[35]M. Watanabe, T. Hayashi, H. Yagasaki, and S. Sasaki, Int. J. Mod. Phys. B **15**, 3997 (2001).
[36]H. Tang, H. Berger, P. E. Schmid, and F. Levi, Solid State Commun. **92**, 267 (1994).
[37]A. Konrad, U. Herr, R. Tidecks, F. Kummer, and K. Samwer, J. Appl. Phys. **90**, 3516 (2001).
[38]K. S. Song and R. T. Williams, *Self-Trapped Excitons* (Springer, Berlin, 1993), p. 410.

Downloaded 17 Oct 2012 to 62.141.173.103. Redistribution subject to AIP license or copyright; see http://jap.aip.org/about/rights_and_permissions

[39]L. Shay and J. H. Wernick, *Ternary Chalcopyrite Semiconductors: Growth, Electronic Properties, and Applications* (Pergamon, New York, 1975), p. 168.
[40]T. V. Perevalov, O. E. Tereshenko, V. A. Gritsenko, V. A. Pustovarov, A. P. Yelisseyev, C. Park, J. H. Han, and C. Lee, J. Appl. Phys. **108**, 013501 (2010).
[41]A. M. Zaitsev, *Optical Properties of Diamond: A Data Handbook* (Springer, Berlin, 2001), p. 500.
[42]C. C. Yeh, T. P. Ma, N. Ramaswamy, N. Rocklein, D. Gealy, T. Graettinger, and K. Min, Appl. Phys. Lett. **91**, 113521 (2007).
[43]P. R. C. Kent and A. Zunger, Phys. Rev. Lett. **86**, 2613 (2001); Phys. Rev. B **64**, 115208 (2001).

Downloaded 17 Oct 2012 to 62.141.173.103. Redistribution subject to AIP license or copyright; see http://jap.aip.org/about/rights_and_permissions